HHS Public Access
Author manuscript
Bone. Author manuscript; available in PMC 2019 April 01.

Published in final edited form as:
Bone. 2018 April ; 109: 49–55. doi:10.1016/j.bone.2018.01.034.

High-frequency spectral ultrasound imaging (SUSI) visualizes early post-traumatic heterotopic ossification (HO) in a mouse model

Kavitha Ranganathan[b,*], **Xiaowei Hong**[b,*], **David Cholok**[a], **Joe Habbouche**[a], **Caitlin Priest**[a], **Christopher Breuler**[a], **Michael Chung**[a], **John Li**[a], **Arminder Kaura**[a], **Hsiao Hsin Sung Hsieh**[a], **Jonathan Butts**[a], **Serra Ucer**[a], **Ean Schwartz**[a], **Steven R. Buchman**[a], **Jan P. Stegemann**[b], **Cheri X. Deng**[b,c], and **Benjamin Levi**[a]

[a]Department of Surgery, University of Michigan, Ann Arbor, MI, USA

[b]Department of Biomedical Engineering, University of Michigan, Ann Arbor, MI, USA

[c]Department of Mechanical Engineering, University of Michigan, Ann Arbor, MI, USA

Abstract

PURPOSE—Early treatment of heterotopic ossification (HO) is currently limited by delayed diagnosis due to limited visualization at early time points. In this study, we validate the use of spectral ultrasound imaging (SUSI) in an animal model to detect HO as early as one week after burn tenotomy.

METHODS—Concurrent SUSI, micro CT, and histology at 1, 2, 4, and 9 weeks post-injury were used to follow the progression of HO after an Achilles tenotomy and 30% total body surface area burn (n=3-5 limbs per time point). To compare the use of SUSI in different types of injury models, mice (n=5 per group) underwent either burn/tenotomy or skin incision injury and were imaged using a 55 MHz probe on VisualSonics VEVO 770 system at one week post injury to evaluate the ability of SUSI to distinguish between edema and HO. Average acoustic concentration (AAC) and average scatterer diameter (ASD) were calculated for each ultrasound image frame. Micro CT was used to calculate the total volume of HO. Histology was used to confirm bone formation.

RESULTS—Using SUSI, HO was visualized as early as 1 week after injury. HO was visualized earliest by 4 weeks after injury by micro CT. The average acoustic concentration of HO was 33% more than that of the control limb (n = 5). Spectroscopic foci of HO present at 1 week that persisted throughout all time points correlated with the HO present at 9 weeks on micro CT imaging.

CONCLUSION—SUSI visualizes HO as early as one week after injury in an animal model. SUSI represents a new imaging modality with promise for early diagnosis of HO.

Corresponding Author and Address for Reprints: Benjamin Levi, M.D., Burn Wound and Regenerative Medicine Laboratory, 1150 W. Medical Center Dr., Ann Arbor, MI 48109, blevi@med.umich.edu, Phone: 734-936-0034, Fax: 734-763-6199.
*indicates equal contribution and co-authorship

Keywords

Heterotopic ossification; spectral ultrasound imaging; quantitative ultrasound; Achilles tenotomy; burn injury; micro CT

Introduction

Patients with severe burns, spinal cord injuries, and orthopedic interventions are at significant risk for developing heterotopic ossification (HO).[1–3] More than65% of major combat injuries and over 10% of patients who undergo invasive joint surgery develop HO.[4] Animal models of traumatic HO have been tailored to create reproducible HO after polytrauma.[5,6] Current treatment strategies are lacking, and even after a technically successful surgical extirpation, over 75% of patients have difficulty maintaining their range of motion.[7] The disruption of physiological structures by HO results in significant morbidity including limited range of motion, pain, and disability in performing activities of daily living.[4,5] Currently, a definitive diagnosis of HO relies on the use of CT and MRI to locate and visualize ectopic lesions.[2,3] Unfortunately, however, these imaging modalities are expensive, and diagnosis is oftentimes delayed as HO is only visualized after it has already formed and matured. In these cases, the critical therapeutic window for non-operative treatment has passed and surgery becomes the only definitive option.[6] Unfortunately, however, surgery is limited by incomplete restoration of range of motion and frequent recurrence in approximately 50-90% of cases.[1]

The early diagnosis of HO is critically important for multiple reasons.[7] Recent studies have analyzed newer strategies to detect early HO in congenital and traumatic forms.[8–10] With improved diagnostic technologies for patients who are at high risk for HO, patients with severe burns and blast injuries may be candidates for medical management as opposed to surgical intervention; more specifically, identifying a technology that can detect HO within 1-3 weeks after initiation will enable the implementation of pharmacologic strategies for early treatment instead of surgery.[8] In animal models, the pharmacologic modulation of BMP signaling demonstrated the greatest reduction in HO when administered 0-2 weeks after injury, and less effect when administered 3-6 weeks after injury.[8] Current diagnostic modalities including CT and MRI are inadequate for the early detection of HO; other developing technologies such as Raman spectroscopy are effective in discriminating endochondral bone development, but have yet to be effectively translated to the clinic.[9]

Spectral ultrasound imaging (SUSI), a technique extended from conventional grayscale B-mode ultrasound imaging, retains the non-invasiveness of ultrasound imaging yet is capable of obtaining objective parameters related to the composition and structural properties of tissues based on an already ubiquitous technology.[11–13] While some studies have tested the use of conventional grayscale ultrasound imaging for the detection of HO, it is not surprising that these studies have proven that ultrasound is effective for visualizing HO only once it has already formed or in the presence of limitations in range of motion, rather than at early time points.[14–16] Conventional grayscale ultrasound imaging primarily provides morphological information of tissue cross-sections with millimeters of spatial resolution. SUSI, on the other hand, utilizes calibrated spectra based on radio-frequency backscattered signals to extract parameters that are system- and operator independent; SUSI provides quantitative and objective tissue characterization.[17] Spectral characteristics including acoustic scatter diameter in addition to other spectral parameters enable detection of tissue compositional changes in addition to morphology. These parameters can be mapped to generate specimen-specific reference ranges. Although high frequency ultrasound is not suitable for use in highly mineralized tissues due to limited penetration and attenuation, SUSI represents a unique advancement for the visualization of developing foci of bone in soft tissue such as HO. Given previous results that have validated the use of spectral parameters of quantitative spectral ultrasound imaging in characterizing solid particles in inhomogeneous materials and improving the early detection of pathologies including breast cancer and atherosclerotic plaques, it is possible that this technology will provide value for the early detection of HO.[18,19,20]

In this study, we validate the use of SUSI in the identification of musculoskeletal tissues, and the visualization of ectopic bone at multiple stages of its development in a mouse model of traumatic HO. We investigated the differences in timing between injury and initial detection of HO using SUSI versus the current gold standard of imaging, micro CT. The use of SUSI has the potential to expand the diagnostic options available to patients with HO, and can also enable the use of additional pharmacologic agents against HO in a more timely manner than what is currently possible.

Material and Methods

2.1 Burn injury and Achilles tenotomy models

To evaluate the ability of SUSI to detect HO, we used our validated burn/tenotomy model[19]. Two groups of studies were performed. First, a longitudinal analysis was conducted to compare an injured limb (left) to an uninjured limb (right) as a control (n=5 mice per group). This specific comparison was selected as a correlate to clinical scenarios in which patients commonly present with one injured limb using imaging from the injured side as a comparison to the uninjured side to detect pathology. Longitudinal analysis was conducted to compare the accuracy and timing of detection using SUSI versus micro CT. Additionally, static time point analyses were performed to compare the uninjured limb (right) to the injured limb with HO (left) using SUSI, CT, and histology at 1, 2, 4, and 9 weeks after injury (n=3-5 mice per time point). To perform the burn/tenotomy surgeries, mice were anesthetized using isofluorane and pre-treated with buprenorphine. The dorsum of each mouse was shaved, and a metal block heated to 60˚Celsius was placed at this site for 18 seconds. Next, a pair of scissors was used to make an incision at the site of the Achilles' tendon. Dissection was carried down to visualize the tendon which was then sharply divided. The skin incision was closed with a 4-0 vicryl suture. No injury was performed on the right limb for comparison.

Next, in order to ensure that the hyperechoic foci detected at one week post-injury were HO rather than simple pockets of edema, we compared the findings of SUSI using two different injury models. Animals underwent either burn/tenotomy (n=5) or burn with skin incision without tenotomy (n=5). This skin incision model results in the presence of edema without

HO, and can thus be used to define the ability of SUSI to distinguish between HO and edema at early time points. SUSI was performed at one week post-injury. For animals treated with skin incision only, mice were anesthetized, shaved, and pre-treated with buprenorphine as above. A scissors was used to make a small skin incision at the site of the Achilles' tendon, but the tendon itself was not divided. The skin incision was closed with a 4-0 vicryl suture.

2.2 Ultrasound imaging and data acquisition

Mice were placed on examination stage and anesthetized with 2% isoflurane in oxygen during ultrasound imaging. Animals were placed on the examination stage with similar orientation, and the skin surface was brought to the focus of the ultrasound probe to optimize the imaging quality. Excessive hair surrounding the heel was removed and ultrasound gel was applied on the skin at the site as a coupling agent. Imaging was performed with a high-resolution small animal ultrasound imaging unit, Vevo 770 System (Visualsonics, Toronto, Canada) and a 55-MHz center frequency single element transducer (Vevo 708 scan head; 20-75 MHz -6 dB bandwidth; 30 μm axial resolution; 70 μm lateral resolution; 4.5 mm focal distance; 1.5 mm -6 dB focal depth; 100% transmit power). Both heels of each mouse were imaged with B-mode, 3D scan mode, and radiofrequency mode to acquire backscattered ultrasound signals for SUSI processing. Cross-section images were obtained under B-mode. A 6 mm range around the calcaneus was scanned with a step size of 30 μm, and 3D images were reconstructed. Backscattered radio frequency (RF) signals were acquired using the RF mode with a 200 μm step size and a 5-millimeter scan range. 3D scanning was accomplished with an automated scanning motor on the system with a 30 μm distance between neighboring frames. This non-invasive imaging procedure requires less than 15 min for each imaging site. Grayscale images were reconstructed from the radio-frequency signals.

2.3 High-frequency spectral ultrasound analysis

2.3.1 Grayscale—Grayscale values GS(y, z) and images were computed as previously mentioned.[20] Briefly, raw backscattered RF data was Hilbert transformed to obtain the complex analytical signal p(y, z). Grayscale B-mode images are reconstructed using the logarithm of amplitude envelop the signal. Quantitatively, grayscale values (GS) were determined as the mean absolute value of the signal over the selected region of interest as:

$$GS(y,\ z) = \log_{10}|p(y,\ z)|.$$

2.3.2 Spectral parameters and parametric images—Analysis of the ultrasound power spectrum has been discussed and applied for detecting mineralization in engineered tissue constructs previously.[21] Similar to our previous work on detecting mineralization, we were targeting ossification at the early stage, in which the mineral nuclei in the soft tissue didn't yield multiple backscattering as mature bone and the spherical scatterer assumption can be applied to yield a first-order approximation. The power spectrum of each RF scan line in an image was calculated by taking the Fast Fourier Transform of the segment of signals gated by a hamming window of 0.2 μs sliding with a 0.1 us offset. To remove system-dependence, the power spectrum of the gated signals was calibrated by dividing it by a calibration power spectrum, which was obtained from a perfect reflector (oil-water interface). Spectral parameters slope (m) and mid-band fit (MBF) were determined by using linear regression to the calibrated power spectrum within a -9 dB bandwidth. Microstructural parameters such as the acoustic scatterer diameter, *a*, which represents an effective size of the acoustic scatters in tissue, can be assessed from the spectral parameters including the slope m, the geometry index (n), the center frequency of the imaging transducer (f_c), and bandwidth of the transducer (b), and is given by:

$$a = 2 * \sqrt{0.25n\frac{[b - (1 - \frac{b^2}{4})]}{b^3 f_c^2} - \frac{m}{105.5 f_c}}.$$

Acoustic concentration, which is denoted as CQ^2, a product of scatter concentration and the square of the acoustic impedance of the scatters, depends on MBF, scatterer diameter (a) and a shape dependent factor (E), and is defined as:

$$\mathrm{CQ}^2 = \frac{\exp(0.23\left(MBF - g_1 n - g_2(\frac{a}{2})^2\right))}{Ea^{2(n-1)}},$$

$$g_1\left(f_c, b\right) = 4.34[\ln(f_c\left(1 - \frac{b^2}{4}\right)^{0.5}\left(\frac{2+b}{2-b}\right)^{\frac{1}{b}}) - 1],$$

$$g_2\left(f_c, b\right) = -76.9 f_c^2(3 + \frac{b^2}{4}).$$

The average scatterer diameter (ASD) and average acoustic concentration (AAC) is calculated as the average value of the scatterer size (a), and the acoustic concentration(CQ^2) respectively in the chosen region of interest (ROI). Due to the large span of the CQ^2 values, AAC values are represented in decible scale[22]. The values of the scatterer diameter and the acoustic concentration were assigned to each pixel in the selected ROI and overlaid on the grayscale image to create parametric images representing these parameters.

2.4 Micro-computed tomography

Micro CT was performed at each time point at which SUSI was performed GE Healthcare Biosciences, using 80 kVp, 80 mA, and 1,100 ms exposure). The anatomic and spatial orientation of HO was characterized using a calibrated imaging protocol as previously described. Three-dimensional reconstructions were performed at a threshold of 800 Houndsfield Units using anatomic landmarks and observer identification to quantify and define the original cortical bone structures. This defined bone mineral within the soft tissues was quantified as HO.[23]

2.5 Histological Staining and Image Acquisition

Animals in each respective experimental arm were euthanized following the conclusion of sonographic and radiographic assays. Harvested hind limbs were fixed in 10% formalin for 24 hours at 4°C. Specimens were subsequently decalcified using 4% EDTA for 3 weeks at 4°C, paraffin processed, and cut in 5μm transversely oriented sections. Specimens were then deparaffinized, rehydrated, and stained using H&E and Movat's Pentachrome formulations. Stained slides were imaged using an Olympus Bx-51 microscope equipped with an Olympus DP-70 high-resolution digital camera.[24]

2.6 Statistical test

ROIs in at least 5 frames from each limb were identified using grayscale images and quantified with GS value and spectral parameters. Results were presented as mean ± SEM. Statistical comparisons of parameters between groups and time points were made using Student's t-test for paired samples and the differences were considered significant at a level of $p<0.05$. In our initial pilot study, the average acoustic concentration (AAC; (10*log(mm-3)) of HO was 37.82 ± 2.41 and 29.34 ± 3.81 for control samples. To be able to detect a true difference between these groups with 80 percent certainty using an alpha of .05, at least 4 mice per group are necessary to ensure adequate power. Therefore, five mice per group were included in the subsequent analysis groups.

Results

3.1 The mineral density of post-traumatic HO foci at early time points indicates a composition that is between cartilage and bone as indicated by ASD and AAC

To assess the ability of SUSI to distinguish between various musculoskeletal tissue types, samples of bone, cartilage, tendon, and muscle were imaged *ex vivo* (Figure 1). Clear distinctions between these tissue types were observed with SUSI (Figure 1A). Bone was the most echogenic, with the highest grayscale values (GS), and was also associated with the high acoustic concentration (AAC: 86.3±1.02, 79.2±1.4, 76.8±1.22 dB[mm^{-3}] for femur, calcaneus, and tibia respectively). Fibrocartilage was less echogenic than bone with a lower AAC (49.2±1.34 dB[mm^{-3}]), but was more mineralized than soft tissues such as tendon (39.7±0.4 dB[mm^{-3}]) and muscle (30.2±1.34 dB[mm^{-3}]) (Figure 1B). In particular, HO has a higher AAC and ASD than cartilage, but less than bone. This indicates the HO development at week 1 is at a level of mineralization between the calcaneus and the cartilage. These findings are consistent with histology demonstrating the progression of HO in previous studies.[25,24] Interestingly, although the grayscale values for all tissue types are similar except muscle, the AAC values exhibited much more differences (Figure 1B and 1C). In addition, while the ASD values may be similar (Figure 1C), the tissue types can be easily differentiated by the AAC values, indicating that SUSI is sensitive in detecting the tissue types based on tissue composition. Importantly, SUSI revealed tissue specific signatures of these samples (Figure 1C) based on both ACC and ASD values, with larger scatter size and higher concentration for more mineralized tissues such as bone.

3.2 SUSI differentiates between post-traumatic HO in the injury model versus edema in the skin incision only model

Injured and sham-treated animals were imaged at one-week post-injury to test whether that SUSI was able to distinguish between edema and HO at very early time points during which time these two structures may be mistaken for one another on imaging. Reconstructed grayscale images from the RF data for the two HO models are presented in Figure 2A and 2B. Differences in the two models were also revealed in the parametric images (Figure 2A and 2B). The quantitative results show significantly higher grayscale value, ASD and AAC value in the HO foci (GS: 42.9±1.6, ASD: 29.2±0.8 μm, AAC: 63.2±2.8 dB[mm^{-3}], n = 5) relative to the surrounding edema (GS: 28.7±0.7, ASD: 26.4±0.3 μm, AAC: 37.2±1.5 dB[mm^{-3}], n = 5) in the B/T model. The calcaneus has the highest value in all three parameters (GS: 50.9±2.0, ASD: 31.5±0.7 μm, AAC: 79.2±1.4 dB[mm^{-3}], n = 5). In the skin incision only model, no ROI with high AAC/ASD values were detected. The edema region in the sham-treated limb show similar grayscale, ASD and AAC value as the edema in the injured limb (GS: 28.3±0.6, ASD: 26.8±0.3 μm, AAC: 39.9±0.5 dB[mm^{-3}], n = 3). As shown clearly in the SUSI signature (Figure 2C), our results comparing the burn/tenotomy limb with the skin incision limb demonstrate that SUSI is able to accurately distinguish between two different injury models. Notably, this technology both qualitatively and quantitatively differentiates between edema and HO as early as one week post-injury (Figure 2).

3.3 SUSI visualizes post-traumatic HO foci as early as one week after injury, and demonstrates progression to mature HO over time

We performed serial imaging at 1, 2, 4, and 9 weeks to demonstrate consistency and accuracy of SUSI over time in terms of the ability to identify HO.

As shown in Figure 3, in the control limb (right limb), both skin and calcaneus maintain a high level of ASD and ACC consistently over time. Connective tissue next to the calcaneus is less echogenic, and has a lower ASD (27.1±0.7 μm) and AAC (47.4±1.7 dB[mm^{-3}]) values in the region. No hyperechoic foci are seen at any time points in the uninjured model. However, on the injured side, parametric images demonstrate that the HO foci are present as early as one week after injury, and have much higher ACC and larger ASD compared to the surrounding edema, The AAC value for the HO foci increases from 63.2±2.8 to 67.7±1.3 dB[mm^{-3}] from week 1 to week 9, while the surrounding edema has an AAC value of 37.2±1.5 and 40.5±1.8 dB[mm^{-3}] at week 1 and week 9. This indicates that HO on SUSI is consistently different from edema longitudinally at all time points. Moreover, while the grayscale values are different between the control and HO model at week 9, only the SUSI ACC values are distinct for the control and HO model as early as week 1. Furthermore, the HO foci at week 9 have slightly higher acoustic concentration compared to earlier time points, demonstrating greater mineralization of these tissues with time. In addition, compared to the calcaneus (AAC value of 79.2±1.4 dB[mm^{-3}] at week 1, the HO foci have slightly lower acoustic concentration indicating a less dense mineral density in the HO foci. The progression of HO over time is clearly evident qualitatively based on the evolution of the hyperechoic foci from weeks 1-9 post-injury (Figure 3B-D). Additionally, the presence of hyperechoic foci on SUSI correlates with early cartilage deposits and inflammation on histology.

3.4 SUSI identifies post-traumatic HO 3-5 weeks earlier than micro CT and is consistent with histological findings

Currently, micro CT serves as the gold standard to detect HO. HO is reliably visualized at approximately 4-6 weeks post-injury using micro CT (Figure 4). Histologically, HO begins as small inflammatory infiltrates which subsequently coalesce into uncalcified regions at 1 week, and transition to calcified and uncalcified fibrocartilage islands approximately 3 weeks after the injury. Approximately 4-6 weeks after the initial injury, these networks of cartilage become bone through the process of endochondral ossification. Using SUSI, we were able to visualize ectopic bone within the calcaneal region of each mouse as early as one week after injury (Figure 4A). The findings of SUSI at early time points and late time points correlated with the presence of HO on histology at all time points and on micro CT at 9 weeks (Figure 4B and 4C). Given the known progression of HO from an inflammatory lesion at 1-2 weeks, to cartilage at 3 weeks, and finally HO after 6 weeks, it is likely that SUSI captures the inflammatory foci that ultimately progress to cartilage and bone at later time points. None of the control limbs demonstrated these inflammatory infiltrates or HO according to micro CT or SUSI (Figure 4). 3D reconstructions performed on SUSI demonstrate that HO can be visualized 3-5 weeks earlier than on micro CT.

Discussion

Timely initiation of early medical management strategies against HO remain ineffective due to a lack of diagnostic strategies available to accurately detect and visualize HO within 1-2 weeks of injury. In this study, we validate the use of SUSI for the early detection of HO within one week of inciting injury using two animal models. When compared to more traditional modalities of imaging including micro CT, SUSI visualized and quantified the presence of HO five weeks earlier, consistent with the formation of HO as visualized by histology. The system and operator independent nature and quantitative output of SUSI simplify its use and allows for providers with varying degrees of training to benefit equally from such advancements. As such, based on the result of our *in vivo* testing, we believe that SUSI represents a promising tool to enable the early detection of HO. Earlier detection may enable the initiation of early pharmacologic treatment among high-risk patients to mitigate the need for surgery. Specifically, we forsee this technology being used in burn patients who develop HO in the elbow >90% of the time. Future studies to validate this technology in deeper tissue forms of HO such as hip replacement are needed. To achieve more penetration depth, ultrasound probe with lower center frequency can be used with the cost in imaging resolution, yet the power spectral analysis has been validated with ultrasound center frequency as low as 5 MHz.[17]

Traditional ultrasound imaging alone has been validated as a screening tool to detect ectopic bone among patients with neurogenic HO. For example, Falsetti et al stated that bedside ultrasound is a safe, non-invasive, cost-effective screening tool important for screening patients with acquired forms of brain injury.[26] Importantly, however, one of the main limitations of this study is the lack of generalizability, as one operator performed all measurements in this study precluding the assessment of inter-operator reliability. In this regard, SUSI represents an improvement beyond traditional ultrasound techniques because SUSI obtains parameters from calibrated spectrum which are objective and quantitative; as these parameters are related to the intrinsic properties of tissues, SUSI allows for greater utility and without the need to rely on subjective graphic assessments. Specifically, SUSI provides parameters that represent tissue properties beyond grayscale imaging intensity. As shown in this study, the utility of SUSI is also demonstrated by its ability to perform comprehensive, objective visualizations of microstructural tissue properties to a much greater degree than conventional ultrasound.[27–31] Such objectivity enhances the application and utility of this technology into clinical environments that are currently founded upon principles of clinical judgement and experience. With regards to patients at high risk for HO specifically after burns and blast injuries, targeted forms of screening may be instituted to promote early detection given that the most common sites of HO have been clearly defined in the past. By implementing standardized imaging procedures at these sites specifically, it may be possible to diagnosis HO earlier than current imaging modalities permit. This process may also be broadened to include imaging for symptomatic regions in patients who present with signs concerning for the development of HO.

Conventional B-mode grayscale values are not absolute and dependent on imaging settings and specific systems and interpretation of these images are not absolute and unable to compared with different studies. Therefore, such qualitative results are inevitably subjected to operator variation. SUSI offers a quantitative method that is system- and operator independent because it uses acoustic scatterer diameter (ASD) and acoustic concentration (AAC) extracted from the backscattered signals to distinguish tissue changes within the region of interest of the injured and control limbs as early as possible for HO diagnosis.

While there are limitations to consider, the strength of our findings lies in the identification of a non-invasive technology that detects the presence of HO much earlier than traditional, gold standard modalities commonly used today. Our study is limited by the restrictions imposed on the serial imaging of animals within our institution. To address this, we performed both longitudinal and individual time point analyses to ensure that we were performing serial evaluations from multiple perspectives using both SUSI and micro CT. Consequently, our results demonstrate that SUSI correlated with micro CT at both final and early time points. Additionally, the overall generalizability of our findings can be enhanced by validating the use of SUSI in other musculoskeletal pathologies as well. The theoretical model we applied herein involves assumption of spherical scatterers, which may not be optimal for some tissue types. Nevertheless, this model provides a first order approximation of more complex scatterer geometry. In addition, the spherical sphere assumption provides an effective radius that can be used to describe any given scatterer. For future work, other theoretical models of various scatterer geometry and dimension, will be investigated.[32, 33] Despite these limitations, the use of SUSI to detect early post-traumatic HO is significant. SUSI represents an effective, non-invasive, potentially cost-effective diagnostic strategy that can facilitate the early diagnosis of HO.

Conclusions

In this study, we demonstrate the utility of SUSI in detecting post-traumatic HO as early as one week post-injury in two models. Application of this technology will facilitate the prompt diagnosis of HO based on both quantitative and objective data. Early diagnosis may allow for timely initiation of treatments that may negate the need for surgical intervention in the future. Using quantitative metrics and advanced, yet noninvasive imaging strategies, SUSI represents an important technological advancement for its application to visualizing ectopic bone formation.

Acknowledgments

Kavitha Ranganathan supported by F32 AR068902-02

BL: Supported by funding from NIH/National Institute of General Medical Sciences Grant K08GM109105, NIH R01GM123069, NIH1R01AR071379, American Association of Plastic Surgery Academic Scholarship and joint PSF Pilot Award, Association for Academic Surgery Roslyn Award, American Association for the Surgery of Trauma Research & Education Foundation Scholarship, International FOP Association

BL collaborated on a project unrelated to this manuscript with Boehringer Ingelheim

JPS, XH, and CXD: supported by funding from NIH R01DE026630

Abbreviations

HO	Heterotopic ossification
SUSI	Spectral ultrasound imaging
B/T	Burn/tenotomy
GS	grayscale
ASD	Average scatterer diameter
AAC	Average acoustic concentration

References

1. Shehab D, Elgazzar AH, Collier BD. Heterotopic ossification. J Nucl Med. 2002; 43(3):346–353. [PubMed: 11884494]
2. Ranganathan K, Loder S, Agarwal S, et al. Heterotopic Ossification: Basic-Science Principles and Clinical Correlates. The Journal of bone and joint surgery American volume. 2015; 97(13):1101–1111. [PubMed: 26135077]
3. Vanden Bossche L, Vanderstraeten G. Heterotopic ossification: a review. Journal of rehabilitation medicine. 2005; 37(3):129–136. [PubMed: 16040468]
4. Potter BK, Burns TC, Lacap AP, Granville RR, Gajewski DA. Heterotopic ossification following traumatic and combat-related amputations. Prevalence, risk factors, and preliminary results of excision. J Bone Joint Surg Am. 2007; 89(3):476–486. [PubMed: 17332095]
5. Peterson JR, Okagbare PI, De La Rosa S, et al. Early detection of burn induced heterotopic ossification using transcutaneous Raman spectroscopy. Bone. 2013; 54(1):28–34. [PubMed: 23314070]
6. Pavey GJ, Qureshi AT, Hope DN, et al. Bioburden Increases Heterotopic Ossification Formation in an Established Rat Model. Clinical orthopaedics and related research. 2015

7. Hunt JL, Arnoldo BD, Kowalske K, Helm P, Purdue GF. Heterotopic ossification revisited: a 21-year surgical experience. J Burn Care Res. 2006; 27(4):535–540. [PubMed: 16819361]
8. Onat SS, Ozisle Z, Orhan A, Akman B, Koklu K, Ozcakar L. Ultrasonographic diagnosis of heterotopic ossification and secondary nerve entrapments in a patient with spinal cord injury. Med Ultrason. 2017; 19(3):338–339. [PubMed: 28845506]
9. Eekhoff EMW, Botman E, Coen Netelenbos J, et al. [18F]NaF PET/CT scan as an early marker of heterotopic ossification in fibrodysplasia ossificans progressiva. Bone. 2017
10. Al Mukaddam M, Rajapakse CS, Pignolo RJ, Kaplan FS, Smith SE. Imaging assessment of fibrodysplasia ossificans progressiva: Qualitative, quantitative and questionable. Bone. 2017
11. Gudur M, Rao RR, Hsiao YS, Peterson AW, Deng CX, Stegemann JP. Noninvasive, Quantitative, Spatiotemporal Characterization of Mineralization in Three-Dimensional Collagen Hydrogels Using High-Resolution Spectral Ultrasound Imaging. Tissue Eng Part C-Me. 2012; 18(12):935–946.
12. Gudur MSR, Rao RR, Peterson AW, Caldwell DJ, Stegemann JP, Deng CX. Noninvasive Quantification of In Vitro Osteoblastic Differentiation in 3D Engineered Tissue Constructs Using Spectral Ultrasound Imaging. PloS one. 2014; 9(1)
13. Deng CX, Hong XW, Stegemann JP. Ultrasound Imaging Techniques for Spatiotemporal Characterization of Composition, Microstructure, and Mechanical Properties in Tissue Engineering. Tissue Eng Part B-Re. 2016; 22(4):311–321.
14. Rosteius T, Suero EM, Grasmucke D, et al. The sensitivity of ultrasound screening examination in detecting heterotopic ossification following spinal cord injury. Spinal cord. 2017; 55(1):71–73. [PubMed: 27349610]
15. Ohlmeier M, Suero EM, Aach M, Meindl R, Schildhauer TA, Citak M. Muscle localization of heterotopic ossification following spinal cord injury. The spine journal : official journal of the North American Spine Society. 2017
16. Stefanidis K, Brindley P, Ramnarine R, et al. Bedside Ultrasound to Facilitate Early Diagnosis and Ease of Follow-Up in Neurogenic Heterotopic Ossification: A Pilot Study From the Intensive Care Unit. The Journal of head trauma rehabilitation. 2017
17. Lizzi FL, Feleppa EJ, Alam SK, Deng CX. Ultrasonic spectrum analysis for tissue evaluation. Pattern Recogn Lett. 2003; 24(4-5):637–658.
18. O'Donnell M, Mimbs JW, Miller JG. Relationship between collagen and ultrasonic backscatter in myocardial tissue. The Journal of the Acoustical Society of America. 1981; 69(2):580–588. [PubMed: 7462481]
19. Sethuraman S, Amirian JH, Litovsky SH, Smalling RW, Emelianov SY. Spectroscopic intravascular photoacoustic imaging to differentiate atherosclerotic plaques. Optics express. 2008; 16(5):3362–3367. [PubMed: 18542427]
20. Banihashemi B, Vlad R, Debeljevic B, Giles A, Kolios MC, Czarnota GJ. Ultrasound imaging of apoptosis in tumor response: novel preclinical monitoring of photodynamic therapy effects. Cancer research. 2008; 68(20):8590–8596. [PubMed: 18922935]
21. Gudur MS, Rao RR, Peterson AW, Caldwell DJ, Stegemann JP, Deng CX. Noninvasive quantification of in vitro osteoblastic differentiation in 3D engineered tissue constructs using spectral ultrasound imaging. PloS one. 2014; 9(1):e85749. [PubMed: 24465680]
22. Oelze ML, O'Brien WD Jr, Blue JP, Zachary JF. Differentiation and characterization of rat mammary fibroadenomas and 4T1 mouse carcinomas using quantitative ultrasound imaging. IEEE Trans Med Imaging. 2004; 23(6):764–771. [PubMed: 15191150]
23. Peterson JR, De La Rosa S, Sun H, et al. Burn injury enhances bone formation in heterotopic ossification model. Annals of surgery. 2014; 259(5):993–998. [PubMed: 23673767]
24. Agarwal S, Loder S, Brownley C, et al. Inhibition of Hif1alpha prevents both trauma-induced and genetic heterotopic ossification. Proceedings of the National Academy of Sciences of the United States of America. 2016; 113(3):E338–347. [PubMed: 26721400]
25. Balboni TA, Gobezie R, Mamon HJ. Heterotopic ossification: Pathophysiology, clinical features, and the role of radiotherapy for prophylaxis. International journal of radiation oncology, biology, physics. 2006; 65(5):1289–1299.

26. Falsetti P, Acciai C, Palilla R, Carpinteri F, Patrizio C, Lenzi L. Bedside ultrasound in early diagnosis of neurogenic heterotopic ossification in patients with acquired brain injury. Clinical neurology and neurosurgery. 2011; 113(1):22–27. [PubMed: 20863614]
27. Insana, MF., B, DG. Acoustic scattering theory applied to soft biological tissue. Boca Raton: CRC Press; 1993.
28. Lizzi FL, Greenebaum M, Feleppa EJ, Elbaum M, Coleman DJ. Theoretical framework for spectrum analysis in ultrasonic tissue characterization. The Journal of the Acoustical Society of America. 1983; 73(4):1366–1373. [PubMed: 6853848]
29. Lizzi FL, Astor M, Feleppa EJ, Shao M, Kalisz A. Statistical framework for ultrasonic spectral parameter imaging. Ultrasound in medicine & biology. 1997; 23(9):1371–1382. [PubMed: 9428136]
30. Lizzi FL, Astor M, Liu T, Deng C, Coleman DJ, Silverman RH. Ultrasonic spectrum analysis for tissue assays and therapy evaluation. Int J Imag Syst Tech. 1997; 8(1):3–10.
31. Berglund JD, Nerem RM, Sambanis A. Viscoelastic testing methodologies for tissue engineered blood vessels. Journal of biomechanical engineering. 2005; 127(7):1176–1184. [PubMed: 16502660]

Highlights

- Acoustic concentration from SUSI correlates with mineralization in different types of tissue.
- SUSI visualizes heterotopic bone formation as early as one-week post injury in a mouse model of traumatic HO.
- HO foci exhibit significantly higher acoustic concentration and scatterer size than surrounding foci of edema.
- SUSI monitors longitudinal progression of HO noninvasively, and correlates with histology and micro CT imaging.

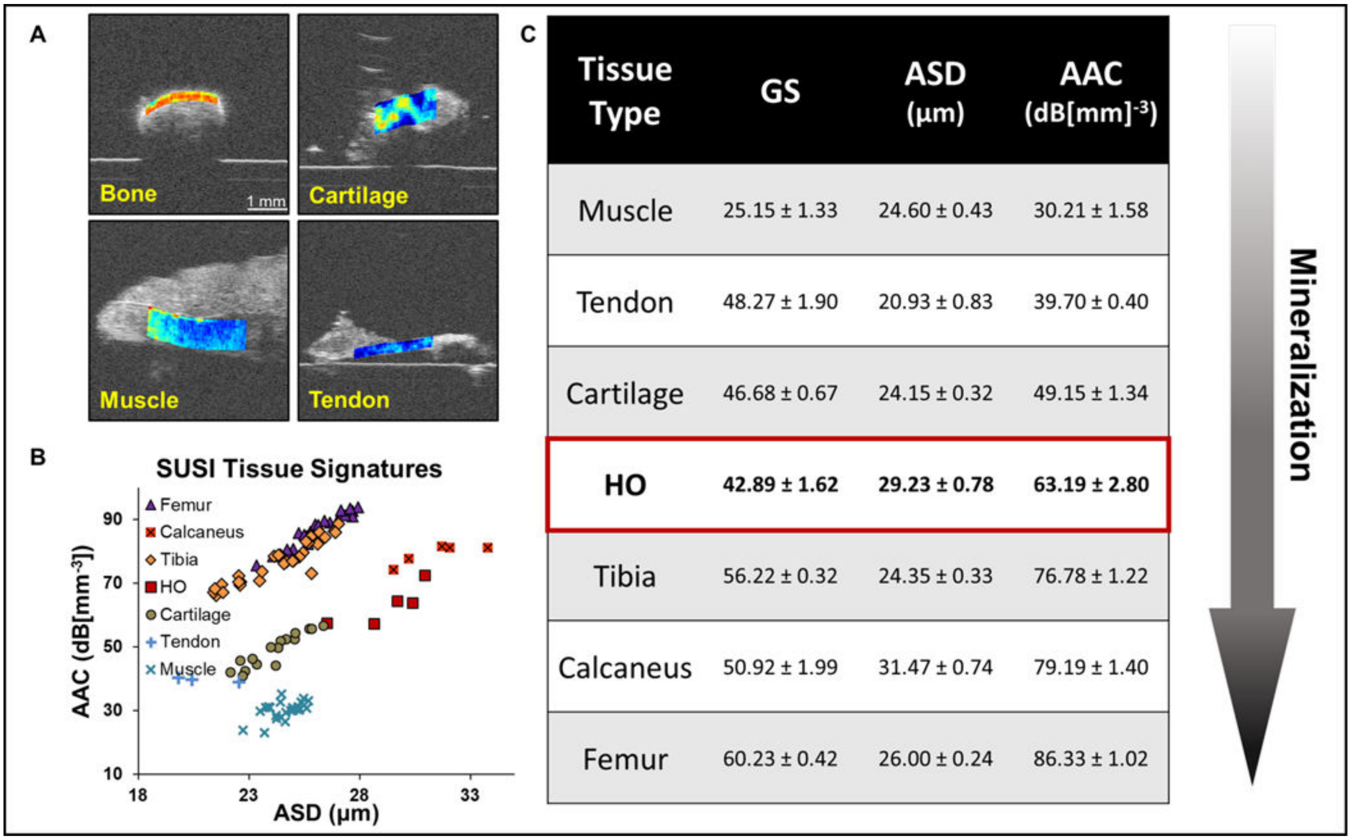

Tissue Type	GS	ASD (μm)	AAC (dB[mm]$^{-3}$)
Muscle	25.15 ± 1.33	24.60 ± 0.43	30.21 ± 1.58
Tendon	48.27 ± 1.90	20.93 ± 0.83	39.70 ± 0.40
Cartilage	46.68 ± 0.67	24.15 ± 0.32	49.15 ± 1.34
HO	**42.89 ± 1.62**	**29.23 ± 0.78**	**63.19 ± 2.80**
Tibia	56.22 ± 0.32	24.35 ± 0.33	76.78 ± 1.22
Calcaneus	50.92 ± 1.99	31.47 ± 0.74	79.19 ± 1.40
Femur	60.23 ± 0.42	26.00 ± 0.24	86.33 ± 1.02

Figure 1.

Characterization of different types of musculoskeletal tissue by SUSI. A. Grayscale images of calcaneus, cartilage, muscle and tendon overlaid with acoustic concentration values (scale bar: 1 mm). B. Table summarizes the mean ± SEM of grayscale intensity, average scatterer diameter (ASD) and average acoustic concentration (AAC) of various musculoskeletal tissue types (n ≥ 3). Heterotopic ossification at 1 week post injury shows AAC values between cartilage and calcaneus, indicating a mineralization level between the two. C. Scatter plot of the ASD and AAC values of various tissue types. Different tissue types can be differentiated by the AAC values.

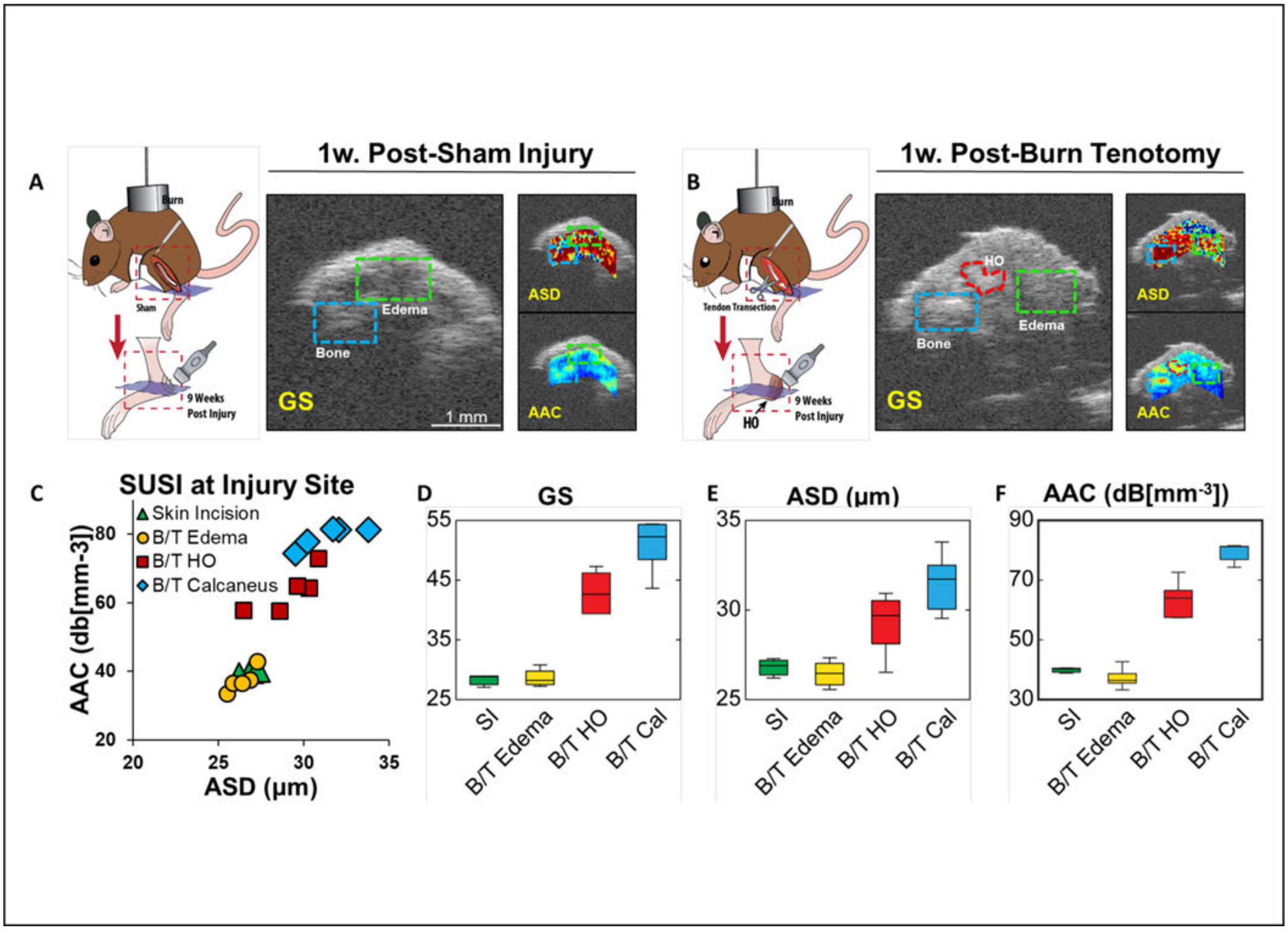

Figure 2.

SUSI comparison of the skin incision (SI) model and the burn/tenotomy model at 1 week post injury. A. As shown in the grayscale image, animal underwent burn and skin incision with tenotomy developed edema (green box) without formation of ectopic bone (scale bar: 1 mm). Low values of AAC are shown in the edema region. B. In animals underwent burn and tenotomy, both edema (green box) and HO (red ROI) formed in the space between bone (blue box) and skin. The HO foci exhibited AAC and ASD values between bone and edema. C. Scatter plot of ASD and AAC values of edema in skin incision model, edema, HO and calcaneus in B/T model (n = 5). D-F. Bar plots of grayscale intensity, ASD and AAC values in the skin incision edema, B/T edema, HO and Calcaneus foci. Edema in both models showed similar ASD and AAC. HO foci showed ASD and AAC values in between edema and bone.

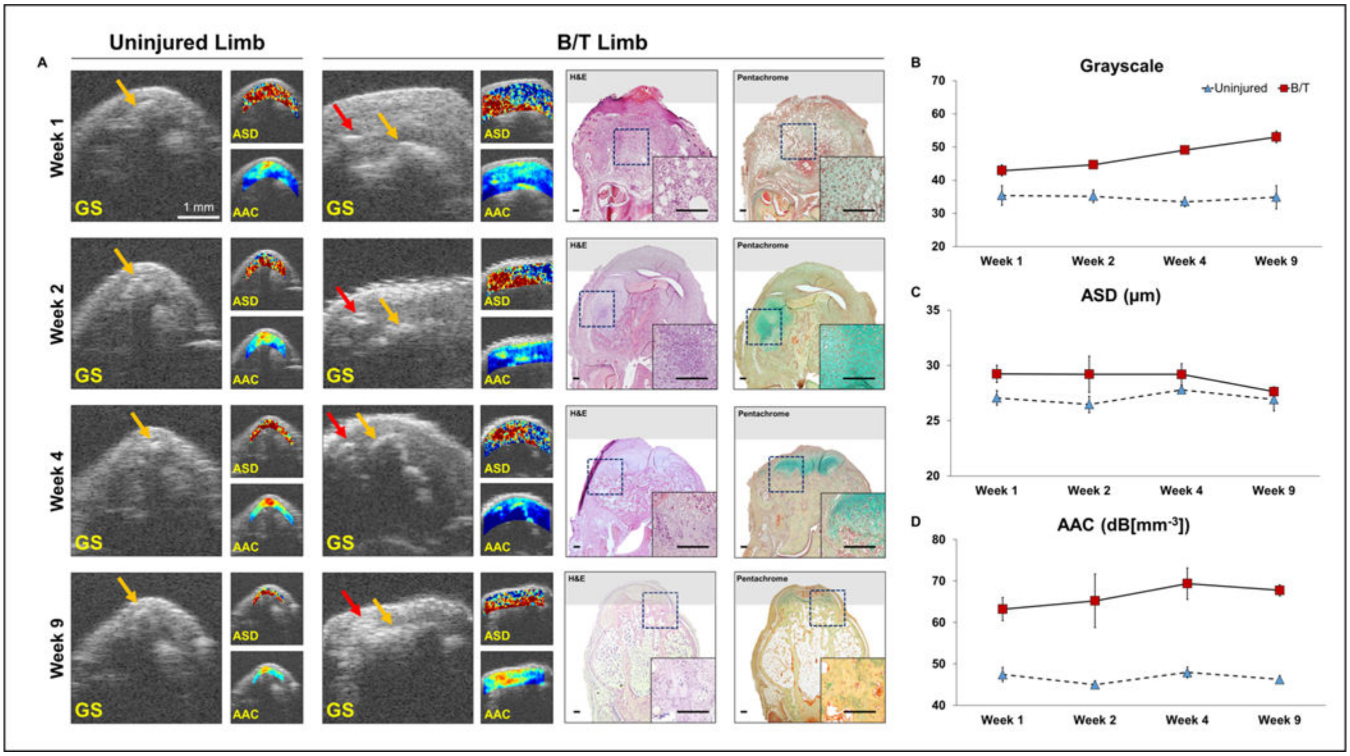

Figure 3.

SUSI monitors longitudinal tissue development in the uninjured and B/T limb at 1, 2, 4 and 9 weeks post injury. A. In the uninjured limb at all four time points, no edema formed and the calcaneus (yellow arrow) was located beneath the skin. In the B/T limb, edema formed and its volume gradually decreased over time (scale bar: 1 mm). HO (red arrow) can be visualized at 1 week post injury. The AAC-overlaid images show high intensity at the bone and HO foci. Corresponding H&E and Pentachrome staining images confirmed the presence of cartilage deposition and inflammation. B-D. Mean ± SEM (n=5) of grayscale intensity, ASD and AAC values are shown for the connective tissue region (between skin and bone) in the uninjured limb, and the HO foci (yellow arrow) in the B/T limb at week 1, 2, 4 and 9 post injury. GS, ASD and AAC values of the HO foci are higher than that in the uninjured limb at all four time points.

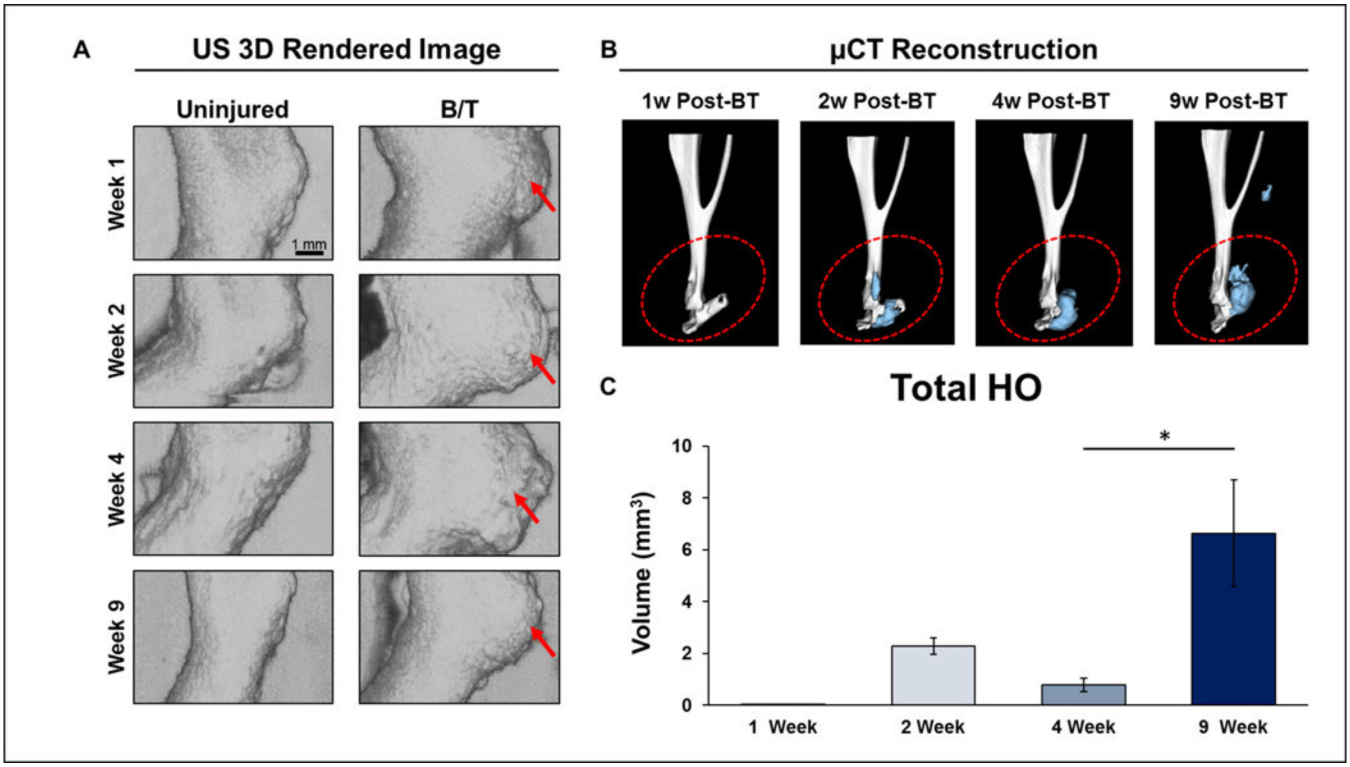

Figure 4.
Concurrent SUSI and micro CT of the uninjured and B/T limbs at 1, 2, 4, and 9 weeks post injury. A. 3D rendered ultrasound images of the uninjured limbs and the B/T limbs (scale bar: 1 mm). Inflammation and HO formation in the B/T were reflected by the tissue volume increase compared to the uninjured limb. B. HO was visualized under micro CT 4 weeks post injury. Blue areas shows the newly formed ectopic bone. C. Mean ± SEM (n=5) of the volume of ectopic bone measured with reconstructed micro CT. Graphic comparison of HO development at 1 week (0.01 ± 0.00 mm^3, n=6), 2 weeks (2.29 ± 0.31 mm^3, n=3), 4 weeks (0.79 ± 0.26 mm^3, n=4), and 9 weeks post-injury (6.64 ± 2.07, n=5). Difference in detectable HO volume at 4 v. 9 weeks is statistically significant (p=0.0465, two-sided student's t-test).